

# Fluorescent Gold Nanoclusters as a Biocompatible Marker for *In Vitro* and *In Vivo* Tracking of Endothelial Cells

Hsueh-Hsiao Wang,<sup>†,‡</sup> Cheng-An J. Lin,<sup>§,¶</sup> Chih-Hsien Lee,<sup>§</sup> Yi-Chun Lin,<sup>†</sup> Ya-Ming Tseng,<sup>†</sup> Chin-Ling Hsieh,<sup>†</sup> Chih-Hao Chen,<sup>†</sup> Cheng-Ho Tsai,<sup>†</sup> Chun-Tai Hsieh,<sup>§</sup> Ji-Lin Shen,<sup>⊥</sup> Wen-Hsiung Chan,<sup>||</sup> Walter H. Chang,<sup>§,¶,\*</sup> and Hung-I Yeh<sup>†,‡,\*</sup>

<sup>†</sup>Departments of Medical Research and Internal Medicine, Mackay Memorial Hospital, Taipei 10449, Taiwan, <sup>‡</sup>Department of Medicine, Mackay Medical College, New Taipei City 252, Taiwan, and Departments of <sup>§</sup>Biomedical Engineering, <sup>⊥</sup>Physics, <sup>||</sup>Bioscience Technology, and <sup>¶</sup>Center for Nano Bioengineering, Chung Yuan Christian University, Chung-Li 32023, Taiwan

Fluorescent probes, with their versatile applications, are widely used for identification and diagnosis in biomedicine. Research of fluorescent molecules aimed at obtaining a strong fluorescent intensity, durable signal, and high biocompatibility, the last property of which is pivotal for their *in vivo* use. Recent advances in nanotechnology have provided platforms for developing nanoscale fluorescent probes, for example, quantum dots.<sup>1</sup> Although compared to traditional fluorescent probes, quantum dots have a stronger fluorescent intensity and a more durable signal. Its use in living cells or animals is limited due to its intrinsic toxicity, which may cause risks to human subjects.<sup>2,3</sup> Molecular clusters of pure metals, especially gold and silver, due to their inert reactivity, have great potential for application in biomedicine. Gold is well-known to be highly biocompatible and has been used in treatments of human inflammatory diseases for a long time.<sup>4,5</sup> Apart from treatment, gold nanoclusters exhibit a potential for the targeted imaging of cancer *in vitro* and *in vivo*.<sup>6,7</sup> Most thiol-related gold nanoclusters protected by glutathione,<sup>8</sup> tiopronin,<sup>9</sup> meso-2,3-dimercaptosuccinic acid,<sup>10</sup> and phenylethylthiolate<sup>11</sup> emit a fluorescence ranging from red to infrared red but have low quantum yields (lower than 1%). In addition to the monolayer-protected nanocluster synthesis, another novel “green” synthetic route for the preparation of red-emitting gold nanoclusters uses bovine serum albumin as the template and reductant.<sup>12</sup> Recently, we developed a novel water-soluble fluorescent gold nanocluster (FANC) with negative-charged surface modification, unique optical property, and a higher

**ABSTRACT** We have been investigating the fluorescent property and biocompatibility of novel fluorescent gold nanoclusters (FANC) in human aortic endothelial cells (HAEC) and endothelial progenitor cells (EPC). FANC (50–1000 nmol/L) was delivered into cells *via* the liposome complex. The fluorescence lasted for at least 28 days with a half-life of 9 days *in vitro*. Examination of 12 transcripts regulating the essential function of endothelial cells after a 72 h delivery showed that only the vascular cell adhesion molecule 1 and the vascular endothelial cadherin were down-regulated at high concentration (500 nmol/L). In addition, no activation of caspase 3 or proliferating cell nuclear antigens was detected. 3-[4,5-Dimethylthiazol-2-yl]-2,5-diphenyltetrazolium bromide (MTT) assay demonstrated that, unlike the markedly suppressed viability in cells treated with quantum dots, FANC had minimal effect on the viability, unless above 500 nmol/L, at which level a minor reduction of viability mainly caused by liposome was found. Tube formation assay showed no impaired angiogenesis in the EPC treated with FANC. *In vivo* study using hindlimb ischemic mice with an intramuscular injection of FANC-labeled human EPC showed that the cells preserved an angiogenic potential and exhibited traceable signals after 21 days. These findings demonstrated that FANC is a promising biocompatible fluorescent probe.

**KEYWORDS:** biocompatibility · endothelial cells · fluorescent gold nanoclusters · *in vitro* test · *in vivo* test · progenitor cells

quantum yield (about 2%).<sup>13</sup> The quantum yield is even improved after thermal treatment. Focus of gold nanoclusters has ranged from its fundamental properties to optional applications. Along with progress in knowledge of gold nanoclusters, major concerns regarding their biomedical use have been brought up because gold nanoparticles had been reported to adversely affect cytoskeleton and viability by interacting with DNA and inducing oxidative stress. However, the biological effect of FANC on the primary cells and animals remains unknown.

To explore the application of FANC *in vivo*, we investigated the fluorescent properties and biocompatibility of FANC in

\* Address correspondence to  
whchang@cycu.edu.tw,  
hiyeh@ms1.mmh.org.tw.

Received for review October 13, 2010  
and accepted May 18, 2011.

Published online May 24, 2011  
10.1021/nn102752a

© 2011 American Chemical Society

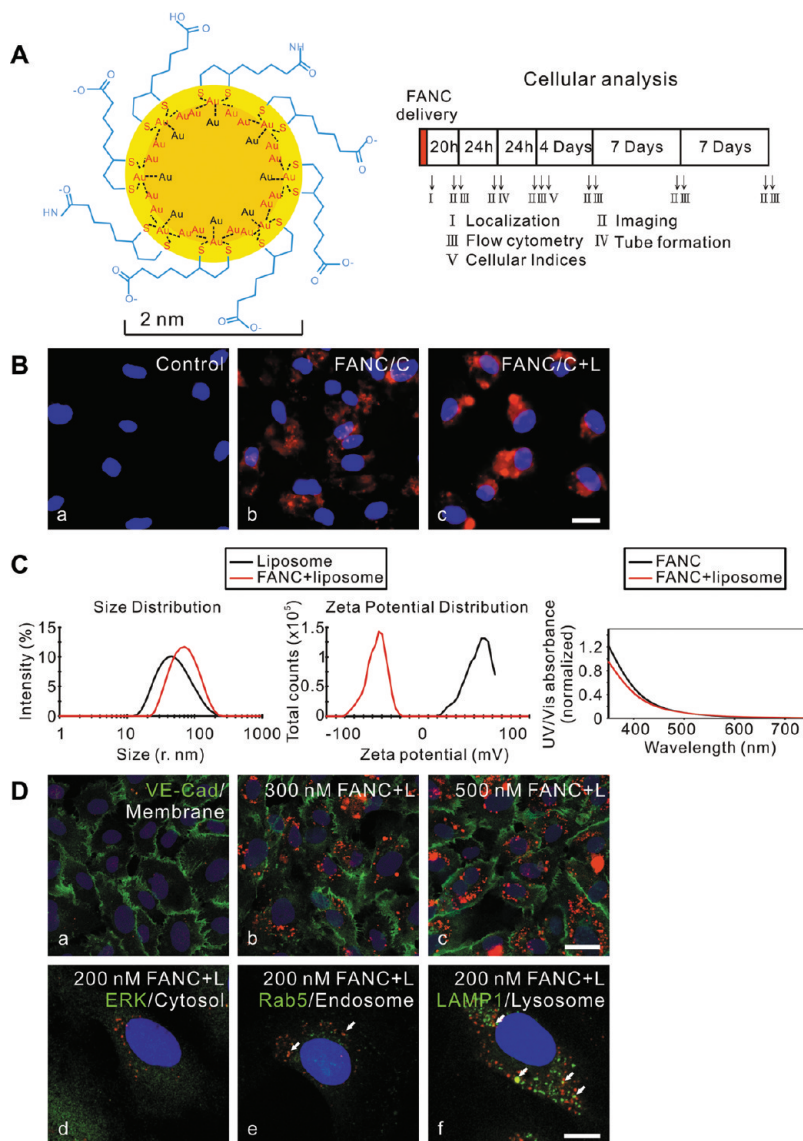


**Figure 1.** Design, delivery, liposome complexation, and subcellular localization of FANC. (A) Schematic diagram shows the time table and approach of *in vitro* analysis. (B) Uptake of FANC, as seen in red fluorescence, was examined using fluorescent microscopy. Cells were treated with 100 nmol/L FANC for 4 h. The blue fluorescence is nucleus-counterstained with bisbenzimid. Control, cells without any treatment; C, serum-free medium; L, in the presence of liposome. (C) Size distribution,  $\zeta$ -potential, and UV-vis absorption spectra of liposome and FANC-liposome complex. (D) After 68 h of recovery, HAEC were fixed and stained with anti-VE-cadherin antibody and bisbenzimid, shown as green and blue labels, respectively. To clarify the subcellular localization of FANC, cells were fixed and stained with antibodies specific to ERK, Rab5, and LAMP1 after 4 h of recovery. Enlarged images of cells with different organelle labeling are shown in panels d–f. The timing for confocal images and concentrations of gold nanoclusters as well as antibodies and their binding organelles are denoted at the top border of each image. Bars, 50  $\mu$ m in B and panels a–c of D, 10  $\mu$ m in panels d–f of D.

human aortic endothelial cells (HAEC). We optimized the delivery of FANC into HAEC and investigated the global cellular indices, including subcellular localization, cell morphology, expression profile, viability, and angiogenic potential. We also examined the effects of FANC on human endothelial progenitor cells (EPC), which originate from peripheral blood mononuclear cells and transform into endothelial cells with high angiogenic properties.<sup>14</sup> The effect of FANC on the angiogenic potential of the EPC was further tested in a murine hindlimb ischemic model. This is the first study

which systematically investigates the biological effect of FANC *in vitro* and *in vivo*.

## RESULTS AND DISCUSSION

**Optimization of Living Cells Labeled with FANC.** Illustrations in Figure 1A show the molecular structure of FANC and design of the *in vitro* experiments of this study. Photophysical characterizations, including the spectra of UV-visible absorption, photoluminescence, and photoluminescence excitation, are shown in Supporting Information Figure 1.<sup>13</sup> A 24 h thermal

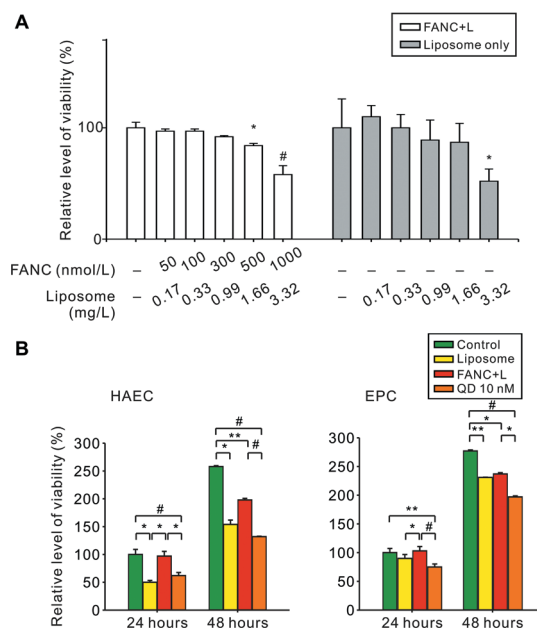


**Figure 2.** Cellular viability of endothelial cells after delivery of FANC and quantum dots (QD). (A) Analysis of the viability in the presence of liposomes (white bars) and liposomes without FANC (gray bars), as evaluated by MTT assay; \*,  $P < 0.05$ ; #,  $P < 0.005$ , compared to the control bar of the same color. (B) Comparison between FANC and QD. Note that both HAEC and EPC treated with FANC exhibit better viability compared to QD. \*,  $P < 0.05$ ; \*\*,  $P < 0.01$ ; #,  $P < 0.005$ .

treatment markedly increased the quantum yield of FANC to nearly 7%, which is favorable for *in vitro* and *in vivo* applications (Supporting Information Figure 2). To test the bioavailability of FANC, HAEC were incubated with 100 nmol/L FANC for 4 h in the absence or presence of liposome in serum-free culture medium (Figure 1B). In the absence of liposome, the cells coated with a conditioned medium exhibited weak red fluorescent signals around the nucleus (Figure 1B, panel b). In contrast, a conditioned medium plus liposome drastically enhanced the delivery efficiency of FANC (Figure 1B, panel c). To evaluate the sustainability of FANC in living cells, HAEC, after 4 h of delivery and different periods of incubation, were examined using fluorescent microscopy. Similar patterns of fluorescent distribution and intensity were observed at different time points (Supporting Information Figure 4, top panel, after 48 h of incubation; bottom panel, after 72 h of incubation). After liposome complexation, the hydrodynamic size of the FANC–liposome complex was increased by 48% (radius of liposome, 43.58 nm; FANC–liposome 64.46 nm), and the  $\zeta$ -potential was shifted negatively from 63 to  $-46$  mV. UV-vis absorption spectra showed that the liposome had minimal effect on FANC (Figure 1C). AFM images of FANC–liposome complexes are shown in Supporting Information Figure 3. Using antibodies specific to VE-cadherin, extracellular signal-regulated kinase (ERK), Rab-protein 5 (Rab5), and lysosomal-associated membrane protein 1 (LAMP1), which respectively labeled the organelles of cell

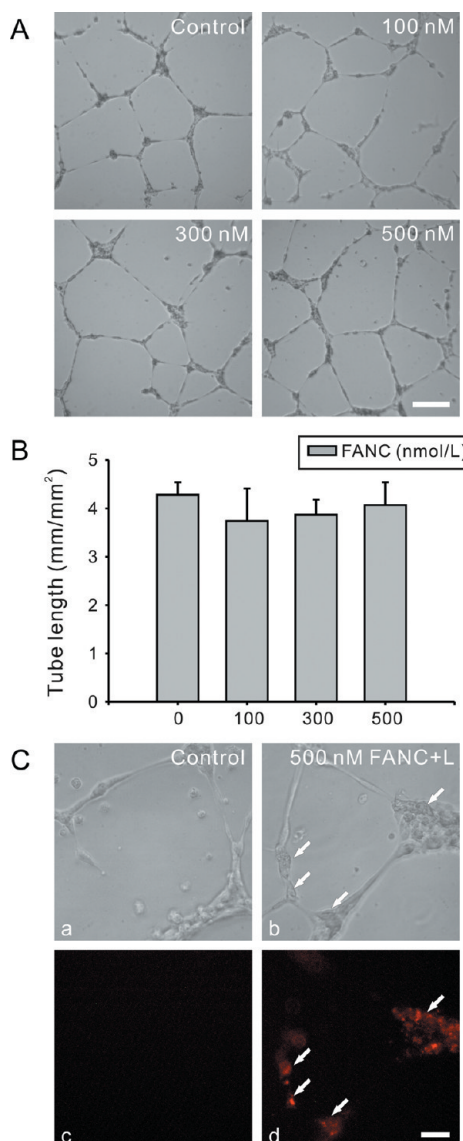


**Figure 3.** Effect of FANC on angiogenic potential. (A) Representative images of HAEC after 24 h of experiment. (B) Tube length was similar between the groups treated with FANC from 100 to 500 nmol/L in the presence of liposome. (C) Visualization of FANC in the polygonal structure of HAEC. Note that a and c, and b and d, respectively, are of the same identical area and c and d are fluorescent images taken using fluorescent microscopy. Arrows in b and d indicate that FANC is located inside the cells. Images in A and C are of the same magnification. Bar, 200  $\mu$ m in A and 50  $\mu$ m in C. Each experiment was performed at least three times in duplicate.

membrane, cytosol, endosome, and lysosome, indicated that cell membranes were negative of FANC labeling (Figure 1D, panels b and c) and FANC mainly existed in cytosol (Figure 1D, panel d). Only part of the FANC signals were colocalized with endosome and lysosome (Figure 1D, panels e and f, indicated by arrows), suggesting that the FANC–liposome complex may enter cells directly. Long-term monitoring showed that the fluorescence signals of FANC-labeled HAEC, though progressively declining in intensity, were easily

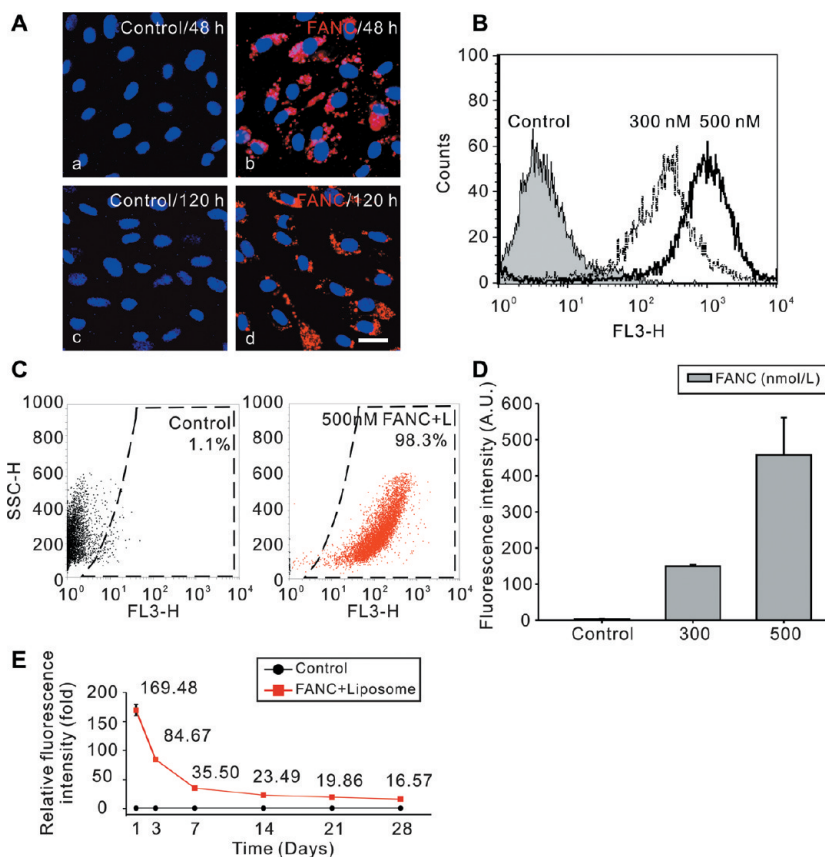


**Figure 4.** Analysis of fluorescence in FANC-labeled human EPCs. (A) Images of FANC-labeled EPCs taken at different time points. (B) After 4 h of FANC delivery and 20 h of recovery, EPCs were trypsinized and subject to flow cytometry analysis. The results showed a dose-dependent increase of the signals. (C) High-labeling efficiency of EPC treated with 500 nM FANC. (D) Quantification of fluorescent intensity in the EPC treated with FANC at different concentrations. (E) Time course of fluorescent intensity in FANC-labeled EPC. Note that in the EPC the fluorescence signals at each time point are all significantly higher, compared to the control groups. Images in A are of the same magnification. Bar, 50  $\mu$ m.

detectable for up to 21 days (Supporting Information Figure 5).

Compared to FANC, quantum dots had a higher fluorescent intensity but much worse biocompatibility in HAEC. Cells treated with quantum dots revealed drastic morphological changes from attached, cobblestone-like to suspended, round-shaped (Supporting Information Figure 6). The results of the FANC delivery showed that serum-depleted mediums enhanced the uptake of FANC, indicating that the autophagic and endocytic pathways induced by nutrition deprivation might facilitate the transfer of FANC, as reported previously.<sup>15,16</sup> Moreover, the addition of liposome into a conditioned medium drastically increased the transport of FANC. Liposome that exhibited the delivery ability in different cell types has been adopted as an effective transporter for macromolecules and other therapeutic agents.<sup>17,18</sup> The present study demonstrates the feasibility of a liposome-based delivery for nanoscale particles.

**Expression Profile of mRNA and Protein in HAEC Labeled with FANC.** After 4 h of FANC delivery and 68 h of incubation, cells were examined with real-time PCR and Western blotting. The transcripts responsible for the essential

functions of endothelial cells, including angiogenesis, vasodilation, coagulation, adhesion, junctional integrity, proliferation, and cytokine expression, were examined (functions of the transcripts are listed in Supporting Information Table 2). Only VE-Cad and VCAM were down-regulated at high concentrations of FANC (decrement at 300 nmol/L, 31% with VCAM, 29% with VE-Cad; at 500 nmol/L, 38% with VCAM, 39% with VE-Cad; all  $P < 0.05$ ; Supporting Information Figure 7). Western blots showed that FANC had no significant effect on the protein level of endothelial markers including Cx43, eNOS, PAI-1, VE-Cad, and KDR (Supporting Information Figure 8). Moreover, caspase 3 activation and PCNA expression in HAEC remained unchanged (Supporting Information Figure 8). The down-regulation of VCAM transcripts by FANC suggested that these nanoscale gold clusters kept a fraction of the innate properties of gold compounds to attenuate the expression profile of cell adhesion molecules.<sup>19</sup> The findings in the present study show that our FANC had minimal effects on caspase 3 activation, and proliferation markers were different from previous studies, which showed that, in endothelial cells, several metal nanoparticles activated the process of apoptosis and attenuated cell proliferation.<sup>20,21</sup>

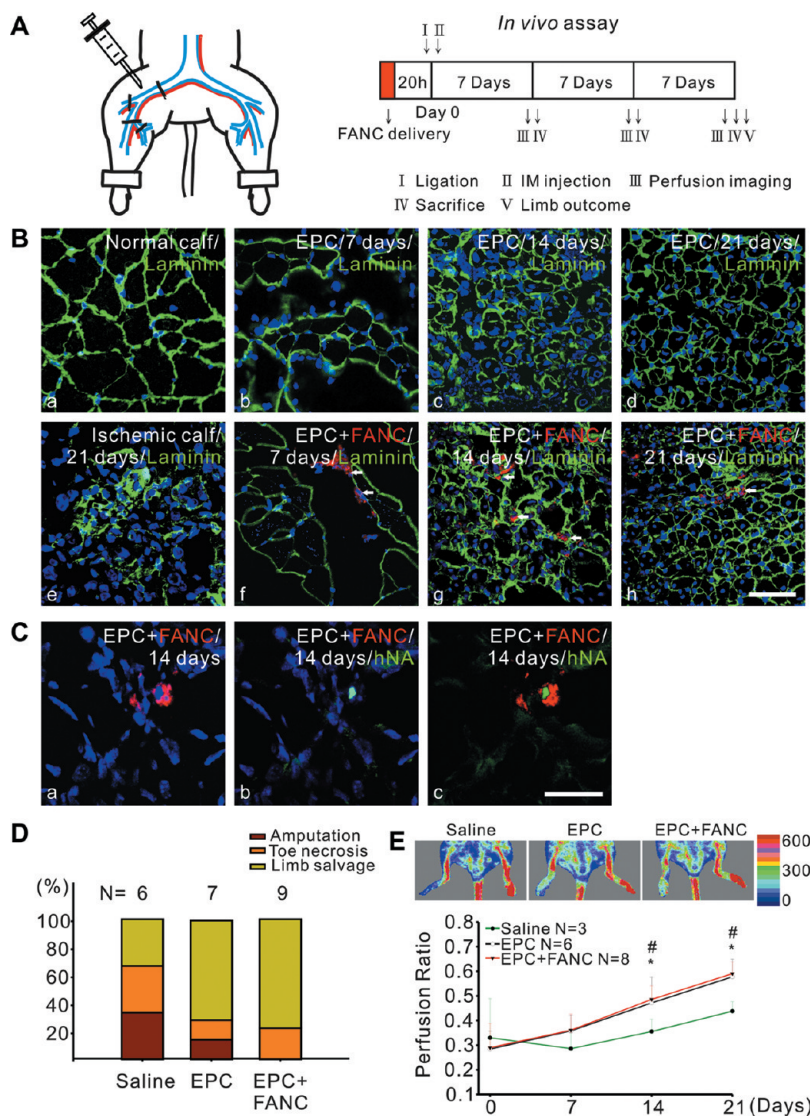


**Figure 5.** *In vivo* tracing of FANC-labeled EPC in hindlimb ischemic mice. (A) Procedures or examinations along the course of *in vivo* assay. Note that the arteries and veins are shown in red and blue, respectively. (B) Confocal images of transverse sections of calf muscles stained with antilaminin antibodies (in green; to outline the structure of myotubes) and bisbenzimidole (in blue; to label the nucleus). Samples were collected from hindlimb ischemic mice injected with EPC labeled with or without FANC (in red; 500 nmol/L in the presence of liposome) at indicated time points. Samples from normal and untreated ischemic tissues were used as controls. Note that FANC-labeled EPCs (arrows) are mainly located at the borders of myotubes. (C) Existence of FANC-labeled human EPCs identified by antihuman nuclear antigens (in green) in calf muscles collected 14 days after vascular ligation. Note that a–c are of the identical area. Red indicates FANC in a and c, while green indicates hNA in b and c. Blue labels are cell nuclei stained with bisbenzimidole. (D) Diagram of limb outcomes 21 days after vascular ligation. (E) Laser-Doppler perfusion imaging at different time points. The recovery in perfusion between groups injected with EPCs or FANC-labeled EPCs is compatible and better than the group injected with saline, on days 14 and 21. \*, P < 0.05, EPC vs saline. #, P < 0.05, EPC+FANC vs saline. Representative images of each group taken at 21 days after vascular ligation are shown here. In the ligated hindlimb (on the left of each image), red indicates more blood flow while blue indicates less or no blood flow. Note that FANC is in red in B and C. All panels in B are of the same magnification. Bars, 45 μm in B; 30 μm in C.

**Biocompatibility of FANC in HAEC Evaluated by Cell Viability and Angiogenic Potential.** Assays of MTT and tube formations were conducted to evaluate the effects of nanoscale gold molecules on cell viability and function because major concerns had been raised regarding the dose-dependent and size-dependent adverse effects of gold nanoparticles on cytoskeleton, field coverage, and viability.<sup>22</sup> In this study, we prepared complexes using a FANC (nmol) to liposome (μg) ratio of 3:10. The MTT assay showed that viability was decreased at the

concentrations above 500 nmol/L of FANC in the presence of liposome (compared to control, 42% decrement at 1000 nmol/L of FANC, which contained 3.32 μg/mL of liposome; Figure 2A, left panel). However, cells treated with liposome only exhibited similar dose-dependent reduction of viability (48% decrement at 3.32 μg/mL; Figure 2A, right panel). Moreover, the viability of cells treated with FANC was better, compared to quantum dots, at both 24 h (decrement of quantum dots, HAEC, 36%; EPC, 27%, Figure 2B) and 48 h (decrement of

quantum dot, HAEC, 33%; EPC, 18%, Figure 2B) after delivery. These findings indicated that FANC was more biocompatible than quantum dots and had no significant effect on viability, the suppression of which seen at concentrations exceeding 500 nmol/L was mainly attributed to the liposome. A previous study also reported that lipid carrier reduced endothelial cell numbers at a concentration of more than 1.6  $\mu\text{g}/\text{mL}$ .<sup>23</sup> Cellular effects of gold nanoparticles, including cell morphology, cytotoxicity, and oxidative stress, may differ according to the surface modifications, size, and treatment concentration.<sup>22,24–26</sup>

The capillary-like tube formation assay showed that, after 48 h of delivery, FANC-labeled HAEC not only built up capillary-like tube structures of an intact patterns but also exhibited visible fluorescent signals in their polygonal structure (Figure 3). The findings indicated that FANC used in the present study do not affect the angiogenic potential of HAEC.

**Evaluation of *In Vivo* Tracking and Angiogenic Potential of Human EPC Labeled with FANC.** After 4 h of FANC delivery and periods of incubation, the pattern of fluorescence in labeled human EPCs was similar to that of labeled HAECs (Figure 4A). To further assess the labeling potency, at 24 h after FANC delivery, human EPCs were examined by flow cytometry, the analysis of which revealed that more than 95% of cells were labeled (Figure 4B,C) and a significant dose-dependent increase of fluorescent intensity existed (increment, 43-fold at 300 nmol/L; 132-fold at 500 nmol/L, compared to control; Figure 4D). Long-term monitoring showed that the fluorescent signal of FANC had a half-life of 9 days in EPCs (Figure 4E and Supporting Information Figure 9). A murine hindlimb ischemic model was used to evaluate the tracking and angiogenic potential of labeled human EPCs (Figure 5A). The results showed that the treatment of EPC or FANC-labeled EPC improved the recovery of myotubes in ischemic mice (Figure 5B, panels b–d and f–h). In addition, FANC-labeled EPCs, with intact nuclei, remained detectable after 21 days of operation (Figure 5B, panels f–h). Anti-hNA staining used to identify human cells showed that hNA is localized to the cells positive for FANC (Figure 5C, panels a–c). Compared to the control group of saline injection, animals injected with human EPC labeled with or without FANC had higher rates of limb salvage (Figure 5D). Consistent with the results of limb outcome, laser–Doppler perfusion imaging showed that both EPC and EPC+FANC groups had increased

subcutaneous blood flows and a higher perfusion ratio on 14 and 21 days after surgery, compared to the saline group (perfusion ratio, respectively, on days 14 and 21, saline, 0.35 and 0.43; EPC, 0.46 and 0.58; EPC+FANC, 0.47 and 0.57; see Figure 5E). These different examinations showed that the effects of EPC and EPC+FANC on the ischemic hindlimb of mice were very much similar.

Regarding fluorescent properties, the broad spectrum of excitation of our FANC not only expanded their applications but also avoided the need for intense light and subsequent phototoxicity in living cells. In addition, red emissions of FANC can be distinguished from tissue green autofluorescence in ischemic organs, which disturbs the interpretation of immunofluorescent microscopy. With a reasonable length of a half-life, high biocompatibility, and limited facilities requirement, FANC has advantages as a tracer over radioactive labeling.<sup>27</sup> Furthermore, the minimal cellular effect shown in the present study and the ability of delivery to different cell types *via* liposome demonstrated that FANC is superior to other agents widely used for cell tracing, such as lipid intercalators PKH,<sup>28,29</sup> carboxy-fluorescein succinimidyl ester (CFSE),<sup>30</sup> and 1,1-dioctadecyl-3,3,3-tetramethylindocarbocyanine perchlorate-acetylated low density lipoprotein (Dil-Ac-LDL);<sup>28,29</sup> the former is susceptible to trypsin digestion, the middle affects cell proliferation and survival at high concentrations,<sup>30,31</sup> and the latter has cell-type selectivity<sup>32</sup> and potential adverse effects.<sup>33</sup> In addition, the red-emitting FANC possesses better penetration but has a lower background in thick tissues.

In this study, with simple procedures, FANC was successfully delivered into HAEC and EPC, which exhibited at least 21 days of fluorescence of dose-dependent intensity. In addition, HAEC exhibiting strong FANC fluorescence was found to have an intact cellular function/expression profile of a wide spectrum, including angiogenesis, vasodilation, coagulation, adhesion, migration, growth, and junctional integrity. Furthermore, *in vitro* and *in vivo* examination of human EPCs showed that the FANC-labeled cells not only exhibited a strong fluorescence but also maintained intact angiogenic potential. All of these findings indicated that FANC is highly biocompatible. FANC may be conjugated to mimic peptides, specific antibodies, or contrast agents for a wider application. In summary, FANC is a promising fluorescent molecule for living cell tracking in biomedical research.

## METHODS

**Preparation of Gold Nanoclusters and Quantum Dots.** Fluorescent gold nanoclusters used in this study were prepared as previously described.<sup>13</sup> Briefly, first, 6 nm gold nanoparticles stabilized with didodecyldimethylammonium bromide (AuNP@DDAB)

were synthesized *via* an established single-phase reaction. Subsequently, further dropwise additions of a gold precursor solution ( $\text{AuCl}_3$  in DDAB/toluene solution) caused a gradual loss of plasmon absorption until the solution turned into a transparent yellowish color. Ligand exchange was performed by

adding the as-prepared nanoclusters to the reduced lipoic acid (DHLA, dihydrolipoic acid), which was freshly reduced by tetrabutylammonium borohydride (TBAB) with a molar ratio of lipoic acid to TBAB = 4:1. This led to dark-brown nanocluster agglomerates in the resulting mixture, and an additional UV lamp exposure (365 nm, 30 min) was treated to condense the agglomerates. After discarding the supernatant, nanoclusters were redispersed in methanol and precipitated again in additional chloroform to remove free surfactants. The dried nanocluster precipitate could be dispersed in borate buffer (pH 9). Further purification was achieved by three runs of ultracentrifugation (110 000 rpm) to remove excess DHLA. Gold nanoclusters were collected, and a PBS buffer was changed through a centrifuge filter of 30 kDa MWCO (molecular weight cutoff), leading to a colloidally stable transparent solution of NCs without a plasmon peak. Twenty-four hours of 70 °C incubation was used to enhance the quantum yields of FANC. Nanoclusters of less stability were precipitated upon centrifugation, leaving well-protected FANC with a decent quantum yield (QE ~7%). Photophysical characterization is shown in the Supporting Information Figures 1 and 2. The concentration of gold nanoclusters was measured by the extinction coefficient to be 450 000 M<sup>-1</sup> cm<sup>-1</sup> at 420 nm. To prepare water-soluble quantum dots, evidot 620 (Evident Technologies, Troy, New York, USA) was coated with amphiphilic polymer<sup>34</sup> followed by 2% agarose gel purification.

**Cell Culture and Fluorescent Au Nanoclusters Delivery.** This investigation conforms with the principles outlined in the Declaration of Helsinki for use of human tissue. Ethical approval was granted by the Institutional Review Board of the Mackay Memorial Hospital, Taipei, Taiwan (reference number: MMH-I-S-566). Human aortic endothelial cells (HAEC) and human CD34-positive endothelial progenitor cells (EPC) were maintained in medium MV and MV2 with growth supplement, respectively (named complete medium; all from PromoCell, Heidelberg, Germany). Isolation, maintenance, and characterization of EPC are described in Supporting Information. The cultures were seeded onto 1% gelatin-coated plasticware or 2% gelatin-coated glass coverslips and maintained in a 37 °C incubator under a humidified 95% air and 5% CO<sub>2</sub> atmosphere. Chemically synthesized gold nanoclusters were delivered into HAEC using complete cultured medium and serum-free medium in the absence or presence of cationic lipid reagent (LipofectAMINE 2000, Invitrogen, Carlsbad, California, USA). Briefly, FANC and liposome were separately diluted in 250 μL of medium without serum and antibiotics. After a 5 min incubation, the diluted FANC and liposomes were gently mixed and incubated for 10 min. The FANC–liposome complexes were further added to plasticware-containing cells and conditioned medium. After 4 h of treatment, media containing gold nanoclusters were replaced with a fresh culture medium. According to the experimental protocols, cells were processed for a real-time polymerase chain reaction, Western blotting, flow cytometry, and cell viability examination, as described in Supporting Information and Methods. To examine the fluorescence of gold nanoclusters, cells were fixed with 2% paraformaldehyde for 10 min, washed with PBS, counterstained with bisbenzimidole (18.7 μmol/L) for 15 min, washed with PBS, and then mounted using 60% glycerol (v/v). To examine the subcellular localization of FANC, antibodies specific to ERK (1:25; Cell Signaling, Danvers, Massachusetts, USA), Rab5 (1:50; Cell Signaling), and LAMP1 (1:20; Abcam, Cambridgeshire, UK) were used. Images were examined by a microscope (DM6000 B, Leica, Wetzlar, Germany) with a 63×/1.32 aperture or 100×/1.40 aperture oil objectives, and the images were captured by a CCD camera (DC 300F, Leica) or scanned by a confocal microscope (TCS SP5, Leica) at room temperature. The scanning parameters are listed in Supporting Information Table 1.

**Analysis of *In Vitro* Angiogenic Potential.** After the delivery of FANC and 20 h of recovery, the cells were trypsinized and resuspended with a medium MV containing 0.5% FBS. Cells were counted by trypan blue staining and diluted to a density of 3 × 10<sup>4</sup> cells/mL. One milliliter of the cell suspension was plated onto a 24-well plate containing 200 μL of solidified Matrigel (Becton Dickinson, Franklin Lakes, New Jersey, USA) per well. Twenty-four hours later, the formation of tube structures was

evaluated. The images were acquired, and the tube length was measured using QWIN image analysis software (Leica) as previously described.<sup>35</sup> For each type of treatment, the cumulative tube length in five randomly selective microscopic fields (40×), derived from three independent experiments, was calculated.

**In Vivo Angiogenesis Model.** This animal investigation conforms with the policies in the Guide for the Care and Use of Laboratory Animals published by the U.S. National Institutes of Health (Publication No. 85-23, revised 1996). The animal-use protocol had been reviewed and approved by the Institutional Animal Care and Use Committee in the Mackay Memorial Hospital, Taipei, Taiwan (reference number: MMH-A-S-7013). To create the hindlimb ischemic model, 8 week old BALB/c female athymic nude mice, weighing 18–22 g, were randomized into three groups. The right femoral artery and vein were ligated and cut from just above the deep femoral artery to the popliteal artery and vein. Twenty four hours after operation, 2 × 10<sup>5</sup> human late EPC in 50 μL of saline were injected into the hindlimb intramuscularly. Animals were sacrificed through intraperitoneal injection of an overdose pentobarbital, and calf muscles were dissected transversally and prepared for immunofluorescent microscopy and histology examination at indicated time points. The structure of myotubes was examined by an antilaminin antibody (1:100, AB2034, Chemicon, Temecula, California, USA). To confirm to the identity of human EPCs, samples blocked with mouse on mouse (MOM) blocking solutions (Vector laboratories, Burlingame, California, USA) were stained by antibodies against human nuclear antigens (hNA; 1:100, MAB1281; Chemicon).<sup>36</sup> All samples were examined under a microscope (DM6000 B, Leica) with a 40×/1.25 aperture oil objective, and the images were captured by a confocal microscope (TCS SP5, Leica) at room temperature.

**Laser-Doppler Perfusion Imaging (LDPI).** Detection of hindlimb subcutaneous blood flow was performed using a laser-Doppler imager (Moor Instruments, Milwae, United Kingdom). Mice were anesthetized with an intraperitoneal injection of pentobarbital (160 mg/kg) and placed on a heater at 37 °C before scanning. The region of interest included the thigh, leg, and foot. Perfusion analyses were performed sequentially at 24 h after surgery (just before the injection of EPC) and at 7, 14, and 21 days after the injection. The calculated perfusion was expressed as a ratio of the left (ischemic) to the right (normal) hindlimb.

**Data Analysis.** Data are expressed as mean ± SD. An analysis was conducted using a one way ANOVA or Student's *t* test. When *P* is valued at <0.05, it is considered statistically significant.

**Acknowledgment.** We gratefully acknowledge the supports of research grants from Taiwan (ROC), The National Science Council (NSC 99-2627-B-033-001, 98-2627-B-195-001, 99-2120-M-038-001, 99-2320-B-033-002 -MY2), The Mackay Memorial Hospital (MMH-E-98003), The Department of Health, Taiwan (DOH 98-TD-N-111-001), and the Specific Research Fields Project of Chung Yuan Christian University (CYCU-98-CR-BE).

**Supporting Information Available:** Supporting methods, photophysical characterization, AFM images, FANC sustainability, comparison between FANC and quantum dots, mRNA transcripts and protein profile analyses, FANC kinetics in living cells, and a list of gene functions. This material is available free of charge via the Internet at <http://pubs.acs.org>.

## REFERENCES AND NOTES

- Jaiswal, J. K.; Matoussi, H.; Mauro, J. M.; Simon, S. M. Long-Term Multiple Color Imaging of Live Cells Using Quantum Dot Bioconjugates. *Nat. Biotechnol.* **2003**, *21*, 47–51.
- Kirchner, C.; Liedl, T.; Kudera, S.; Pellegrino, T.; Munoz Javier, A.; Gaub, H. E.; Stolzle, S.; Fertig, N.; Parak, W. J. Cytotoxicity of Colloidal CdSe and CdSe/ZnS Nanoparticles. *Nano Lett.* **2005**, *5*, 331–338.
- Hardman, R. A Toxicologic Review of Quantum Dots: Toxicity Depends on Physicochemical and Environmental Factors. *Environ. Health Perspect.* **2006**, *114*, 165–172.
- Forestier, J. Copper and Gold Salts in Rheumatoid Arthritis. *Ann. Rheum. Dis.* **1949**, *8*, 132–134.

5. Lehman, A. J.; Esdaile, J. M.; Klinkhoff, A. V.; Grant, E.; Fitzgerald, A.; Canvin, J. A 48-Week, Randomized, Double-Blind, Double-Observer, Placebo-Controlled Multicenter Trial of Combination Methotrexate and Intramuscular Gold Therapy in Rheumatoid Arthritis: Results of the METGO Study. *Arthritis Rheum.* **2005**, *52*, 1360–1370.
6. Retnakumari, A.; Setua, S.; Menon, D.; Ravindran, P.; Muhammed, H.; Pradeep, T.; Nair, S.; Koyakutty, M. Molecular-Receptor-Specific, Non-toxic, Near-Infrared-Emitting Au Cluster-Protein Nanoconjugates for Targeted Cancer Imaging. *Nanotechnology* **2010**, *21*, 055103.
7. Wu, X.; He, X.; Wang, K.; Xie, C.; Zhou, B.; Qing, Z. Ultrasmall Near-Infrared Gold Nanoclusters for Tumor Fluorescence Imaging *In Vivo*. *Nanoscale* **2010**, *2*, 2244–2249.
8. Negishi, Y.; Takasugi, Y.; Sato, S.; Yao, H.; Kimura, K.; Tsukuda, T. Magic-Numbered Au(*n*) Clusters Protected by Glutathione Monolayers (*n* = 18, 21, 25, 28, 32, 39): Isolation and Spectroscopic Characterization. *J. Am. Chem. Soc.* **2004**, *126*, 6518–6519.
9. Wang, G.; Huang, T.; Murray, R. W.; Menard, L.; Nuzzo, R. G. Near-IR Luminescence of Monolayer-Protected Metal Clusters. *J. Am. Chem. Soc.* **2005**, *127*, 812–813.
10. Negishi, Y.; Tsukuda, T. Visible Photoluminescence From Nearly Monodispersed Au-12 Clusters Protected by *meso*-2,3-Dimercaptosuccinic Acid. *Chem. Phys. Lett.* **2004**, *383*, 161–165.
11. Lee, D.; Donkers, R. L.; Wang, G.; Harper, A. S.; Murray, R. W. Electrochemistry and Optical Absorbance and Luminescence of Molecule-like Au38 Nanoparticles. *J. Am. Chem. Soc.* **2004**, *126*, 6193–6199.
12. Xie, J.; Zheng, Y.; Ying, J. Y. Protein-Directed Synthesis of Highly Fluorescent Gold Nanoclusters. *J. Am. Chem. Soc.* **2009**, *131*, 888–889.
13. Lin, C. A.; Yang, T. Y.; Lee, C. H.; Huang, S. H.; Sperling, R. A.; Zanella, M.; Li, J. K.; Shen, J. L.; Wang, H. H.; Yeh, H. I.; et al. Synthesis, Characterization, and Bioconjugation of Fluorescent Gold Nanoclusters toward Biological Labeling Applications. *ACS Nano* **2009**, *3*, 395–401.
14. Asahara, T.; Murohara, T.; Sullivan, A.; Silver, M.; van der Zee, R.; Li, T.; Witzenbichler, B.; Schatteman, G.; Isner, J. M. Isolation of Putative Progenitor Endothelial Cells for Angiogenesis. *Science* **1997**, *275*, 964–967.
15. Meijer, A. J.; Codogno, P. Regulation and Role of Autophagy in Mammalian Cells. *Int. J. Biochem. Cell Biol.* **2004**, *36*, 2445–2462.
16. Liou, W.; Geuze, H. J.; Geelen, M. J.; Slot, J. W. The Autophagic and Endocytic Pathways Converge at the Nascent Autophagic Vacuoles. *J. Cell Biol.* **1997**, *136*, 61–70.
17. Delle, H.; Noronha, I. L. Induction of Indoleamine 2,3-Dioxygenase by Gene Delivery in Allogeneic Islets Prolongs Allograft Survival. *Am. J. Transplant* **2010**, *10*, 1918–1924.
18. Martin-Montanez, E.; Lopez-Tellez, J. F.; Acevedo, M. J.; Pavia, J.; Khan, Z. U. Efficiency of Gene Transfection Reagents in NG108-15, SH-SY5Y and CHO-K1 Cell Lines. *Methods Find. Exp. Clin. Pharmacol.* **2010**, *32*, 291–297.
19. Tozawa, K.; Kawai, N.; Hayashi, Y.; Sasaki, S.; Kohri, K.; Okamoto, T. Gold Compounds Inhibit Adhesion of Human Cancer Cells to Vascular Endothelial Cells. *Cancer Lett.* **2003**, *196*, 93–100.
20. Park, E. J.; Yi, J.; Chung, K. H.; Ryu, D. Y.; Choi, J.; Park, K. Oxidative Stress and Apoptosis Induced by Titanium Dioxide Nanoparticles in Cultured BEAS-2B Cells. *Toxicol. Lett.* **2008**, *180*, 222–229.
21. Kalishwaralal, K.; Banumathi, E.; Pandian, S. R.; Deepak, V.; Muniyandi, J.; Eom, S. H.; Gurunathan, S. Silver Nanoparticles Inhibit VEGF Induced Cell Proliferation and Migration in Bovine Retinal Endothelial Cells. *Colloids Surf. B* **2009**, *73*, 51–57.
22. Pernodet, N.; Fang, X.; Sun, Y.; Bakhtina, A.; Ramakrishnan, A.; Sokolov, J.; Ulman, A.; Rafailovich, M. Adverse Effects of Citrate/Gold Nanoparticles on Human Dermal Fibroblasts. *Small* **2006**, *2*, 766–773.
23. Axel, D. I.; Spyridopoulos, I.; Riessen, R.; Runge, H.; Viebahn, R.; Karsch, K. R. Toxicity, Uptake Kinetics and Efficacy of New Transfection Reagents: Increase of Oligonucleotide Uptake. *J. Vasc. Res.* **2000**, *37*, 221–234.
24. Pan, Y.; Neuss, S.; Leifert, A.; Fischler, M.; Wen, F.; Simon, U.; Schmid, G.; Brandau, W.; Jähnen-Dechent, W. Size-Dependent Cytotoxicity of Gold Nanoparticles. *Small* **2007**, *3*, 1941–1949.
25. Yen, H. J.; Hsu, S. H.; Tsai, C. L. Cytotoxicity and Immunological Response of Gold and Silver Nanoparticles of Different Sizes. *Small* **2009**, *5*, 1553–1561.
26. Pan, Y.; Leifert, A.; Ruau, D.; Neuss, S.; Bornemann, J.; Schmid, G.; Brandau, W.; Simon, U.; Jähnen-Dechent, W. Gold Nanoparticles of Diameter 1.4 nm Trigger Necrosis by Oxidative Stress and Mitochondrial Damage. *Small* **2009**, *5*, 2067–2076.
27. Aicher, A.; Brenner, W.; Zuhayra, M.; Badorff, C.; Massoudi, S.; Assmus, B.; Eckey, T.; Henze, E.; Zeiher, A. M.; Dimmeler, S. Assessment of the Tissue Distribution of Transplanted Human Endothelial Progenitor Cells by Radioactive Labeling. *Circulation* **2003**, *107*, 2134–2139.
28. Aoki, M.; Yasutake, M.; Murohara, T. Derivation of Functional Endothelial Progenitor Cells from Human Umbilical Cord Blood Mononuclear Cells Isolated by a Novel Cell Filtration Device. *Stem Cells* **2004**, *22*, 994–1002.
29. Iwaguro, H.; Yamaguchi, J.; Kalka, C.; Murasawa, S.; Masuda, H.; Hayashi, S.; Silver, M.; Li, T.; Isner, J. M.; Asahara, T. Endothelial Progenitor Cell Vascular Endothelial Growth Factor Gene Transfer for Vascular Regeneration. *Circulation* **2002**, *105*, 732–738.
30. Quah, B. J.; Warren, H. S.; Parish, C. R. Monitoring Lymphocyte Proliferation *In Vitro* and *In Vivo* with the Intracellular Fluorescent Dye Carboxyfluorescein Diacetate Succinimidyl Ester. *Nat. Protoc.* **2007**, *2*, 2049–2056.
31. Hemmrich, K.; Meersch, M.; von Heimburg, D.; Pallua, N. Applicability of the Dyes CFSE, CM-Dil and PKH26 for Tracking of Human Preadipocytes To Evaluate Adipose Tissue Engineering. *Cells Tissues Organs* **2006**, *184*, 117–127.
32. Gaffney, J.; West, D.; Arnold, F.; Sattar, A.; Kumar, S. Differences in the Uptake of Modified Low Density Lipoproteins by Tissue Cultured Endothelial Cells. *J. Cell. Sci.* **1985**, *79*, 317–325.
33. Devries-Seimon, T.; Li, Y.; Yao, P. M.; Stone, E.; Wang, Y.; Davis, R. J.; Flavell, R.; Tabas, I. Cholesterol-Induced Macrophage Apoptosis Requires ER Stress Pathways and Engagement of the Type A Scavenger Receptor. *J. Cell Biol.* **2005**, *171*, 61–73.
34. Lin, C. A.; Sperling, R. A.; Li, J. K.; Yang, T. Y.; Li, P. Y.; Zanella, M.; Chang, W. H.; Parak, W. J. Design of an Amphiphilic Polymer for Nanoparticle Coating and Functionalization. *Small* **2008**, *4*, 334–341.
35. Wang, H. H.; Kung, C. I.; Tseng, Y. Y.; Lin, Y. C.; Chen, C. H.; Tsai, C. H.; Yeh, H. I. Activation of Endothelial Cells to Pathological Status by Down-Regulation of Connexin43. *Cardiovasc. Res.* **2008**, *79*, 509–518.
36. Cho, S. W.; Moon, S. H.; Lee, S. H.; Kang, S. W.; Kim, J.; Lim, J. M.; Kim, H. S.; Kim, B. S.; Chung, H. M. Improvement of Postnatal Neovascularization by Human Embryonic Stem Cell Derived Endothelial-like Cell Transplantation in a Mouse Model of Hindlimb Ischemia. *Circulation* **2007**, *116*, 2409–2419.